Characterization of Fusion Welded Ceramics in the SiC-ZrB2-ZrC System

Jecee D. Jarman*, William G. Fahrenholtz*, Greg E. Hilmas*, Jeremy L. Watts*, Derek S. King**

*Materials Science and Engineering Department, Missouri University of Science and Technology, Rolla, Missouri 65409

**UES, Inc. Dayton, Ohio 45432

Corresponding Author: Jecee D. Jarman Email: jjtf7@umsystem.edu Current Address: 2004 Hwy E, Apt D, Rolla, MO 65401

Keywords: joints/joining, phase equilibria, ultra-high temperature ceramics, borides, carbides

NO COLOR NEEDED FOR ANY IMAGES

Abstract:

Various SiC-ZrB₂-ZrC ceramics were joined by fusion welding to determine the maximum silicon carbide content that could be joined. Commercial powders were hot pressed, machined, and preheated to 1450°C before joining with a tungsten inert gas welding torch at 160-200 A. Resulting welds were cross-sectioned and analyzed to determine which compositions were weldable and to characterize microstructural evolution in welded samples. As compositions approached the ternary eutectic, the welds had smaller SiC grains and exhibited better weldability. Penetration depth of welds was controlled by a combination of current input and welding speed. The ternary eutectic in the system was found at 36.9±1.3 vol% SiC, 42.7±1.5 vol% ZrB₂, and 20.4±1.9 vol% ZrC and its melting temperature was 2330±23°C. A ternary phase diagram for the SiC-ZrB₂-ZrC was constructed and proposed via microstructural analysis of arc melted pellets on binary joins between each binary eutectic and the ternary eutectic in the system.

1. Introduction

Silicon carbide (SiC) is touted for its high hardness, strength at elevated temperatures, and chemical inertness. ¹⁻³ In general, monolithic SiC ceramics exhibit a low fracture toughness, but decades of research has been performed to toughen SiC using SiC fiber reinforcements to produce SiC/SiC composites. These composites have shown a desirable range of tailorable strength and toughness values and are candidates for use in aerospace and armor applications. ⁴⁻⁷ Beyond these properties, SiC ceramics possess neutron irradiation tolerance, which has led to growing interest in the nuclear community to consider SiC and SiC/SiC composites as candidates for structural materials in next generation nuclear reactors. ^{2,8-10} To successfully implement SiC/SiC composites into reactors, a dependable joining method is required. Brazing is a commonly used method for joining ceramics and has been shown to successfully join various types of ceramics, including SiC components. ^{11,12} Typically, these SiC joints contained metallic brazes and/or other filler materials that did not possess the same properties as SiC since they were chemically different. Therefore, brazes exhibited problems with neutron irradiation tolerance and remaining inert in nuclear environments. ¹

Fusion welding of ceramics was first described by Rice and is an alternative to brazing that can join ceramic samples with complex geometries. ¹³ Fusion welding relies on melting by a heat source and then recrystallizing the parent material. The heat source can be a laser, an electron beam, or an electric arc, but the material must form a liquid when melted in order to produce a fusion weld. On its own, SiC does not melt at ambient pressure, but decomposes on heating to temperatures around 2500°C. ¹⁴ For this reason, SiC cannot be fusion welded on its own and requires other components to form a liquid during welding. Recently, arc welding of zirconium diboride (ZrB₂) was patented by Hilmas et al. and demonstrated that ultra-high temperature ceramics (UHTCs) could be joined by this method. ¹⁵ King et al. later showed that ZrB₂ and zirconium carbide (ZrC) welds were feasible and soon after produced welded SiC-ZrB₂-ZrC ceramics by utilizing eutectic invariant reactions between SiC, ZrB₂ and ZrC. ¹⁶ This method was able to join a composition consisting of 50 SiC-35 ZrB₂-15 ZrC in volume percent (vol%) through plasma arc welding and pulsed plasma arc welding, without any measurable loss of SiC. The

success of welding was attributed to the high electrical and thermal conductivities of ZrB₂, which are similar to those of weldable metals.¹⁶ Welding of pure ZrB₂, ZrB₂-ZrC, and the SiC-ZrB₂-ZrC ceramics suggests that other compositions in the ternary system can also be welded. Numerous ceramics have been produced in this phase system via spark plasma sintering and arc melting, but to date, no detailed ternary phase diagram has been published for the system.^{17–19} In this work, the SiC-ZrB₂-ZrC system is explored to determine the weldability of compositions within the ternary composition range with an emphasis on maximizing SiC content in the weldable compositions. Experiments were also performed to determine the inflection and approximate locations of the phase boundaries in the SiC-ZrB₂-ZrC system along with the melting temperature of the ternary eutectic.

2. Experimental Procedure

2.1 Batching and Hot-Pressing

The starting powders were commercially available and are listed in Table 1. The batched compositions of SiC, ZrB_2 , and ZrC are listed in Table 2 and plotted, and numbered in Figure 1. After batching each composition, total powder mass was calculated and super-additions of 1 wt% of both B_4C and C (phenolic resin with char yield = 43%) were added to each batch to serve as sintering aids. Attrition milling was used to homogenize the powders and reduce the particle size from "as received" size to ~0.1 to 0.2 μ m to help increase final sintered density. All powder charges were attrition milled with SiC milling media for two hours in acetone and dried by rotary evaporation. The dried powders were ground with a mortar and pestle until they passed through a 200-mesh sieve. Contamination from each milling cycle was measured by measuring the lost mass of the SiC media and used to adjust compositions accordingly.

Table 1: Summary of starting materials.

Material	Grade	Lot	Supplier Impurities (wt%)	Supplier	
a-SiC	UF-25	4114	1.9 O, 0.05 Fe, 0.03 Al	H.C. Starck	
ZrB ₂	В	87298	1.53 Hf, 0.6 O, 0.14 C,	H.C. Starck	
			0.11 N, 0.04 Fe		
ZrC	В	23091/12	2.0 Hf, 0.7 C (free), 0.5 O,	H.C. Starck	
			0.2 N, 0.01 Fe		
B ₄ C	HS	1204/09	1.2 O, 0.2 N, 0.1 Si,	H.C. Starck	
			0.04 Fe, 0.01 Al		
Phenolic	-	-	-	Georgia Pacific	
Resin				Chemicals	

Table 2: Characteristics of compositions tested for weldability including composition, density, and size of SiC grains in the parent material before welding.

Composition in Vol %	Comp.	Bulk Density	Theoretical	SiC Grain Size in
(SiC/ZrB ₂ /ZrC)	Number	(g/cm³)	Density (g/cm³)	Parent Material (μm)
74.3/15.9/9.8	1	3.75	4.00	Not weldable
68.5/19/12.5	2	4.05	4.19	Not weldable
62.8/22.6/14.5	3	4.07	4.35	Not weldable
63.7/14.8/21.5	4	4.15	4.37	Not weldable
57.3/26.2/16.5	5	4.44	4.53	1.3±0.6
52/29.6/18.4	6	4.60	4.69	1.2±0.6
46.9/32.9/20.2	7	4.78	4.85	1.3±0.6
42/36/22	8	4.91	5.00	1.4±0.7
36.3/38.4/25.3	9	5.12	5.18	1.4±0.7
37.8/42.7/19.5	10	5.08	5.11	1.4±0.7

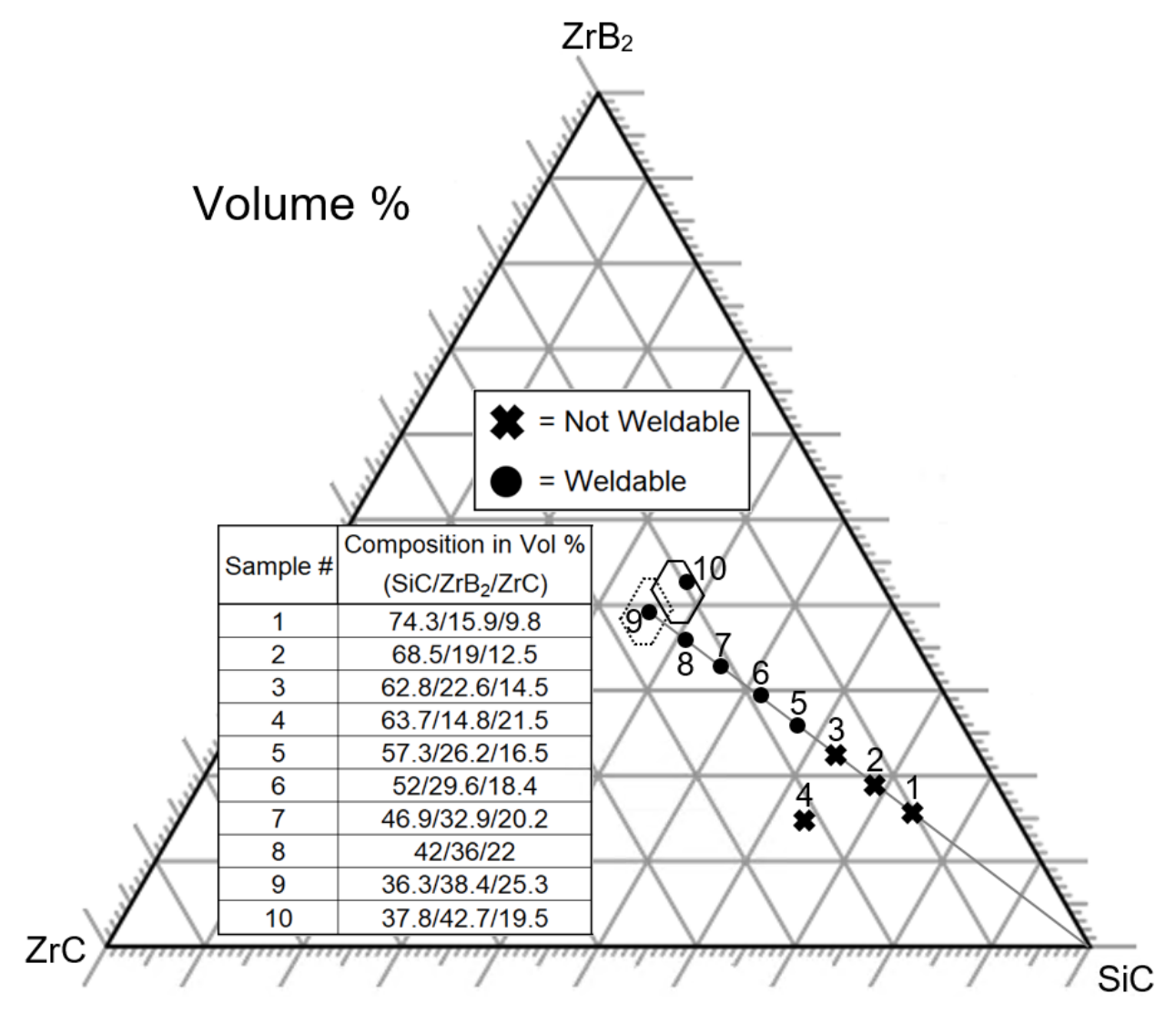


Figure 1: Schematic (vol%) showing batched compositions along a join from SiC to the presumed eutectic composition (hexagon with dotted lines). The solid black hexagon indicated the ternary eutectic area determined in the present study.

Powder mixtures were loaded into either a 25.4 mm round or 47 mm x 31 mm rectangular graphite die (ET-10, Graphite Products, Madison, WI). Dies were lined with two layers of graphite foil (GTA, Gra-foil, Parma, OH). The inner layer of graphite foil was coated using hexagonal BN spray (SP-108, Materion, Milwaukee, WI) to act as a barrier material to prevent reaction between graphite and the ceramic. The prepared graphite die was cold compacted to 5 MPa then loaded into a resistively heated hot press (HP-20, Thermal Technology LLC, Santa Rosa, CA). Specimens were heated at 25°C per minute

with one hour holds at 1450°C and 1650°C under vacuum to promote reactions to remove oxide surface impurities. ^{20, 21} Following these holds, the atmosphere was changed to flowing helium, a pressure of 32 MPa was applied, and the temperature was increased to the final sintering temperature of 2100°C. The pressure and temperature were held until ram travel remained constant for 5 minutes, which indicated that densification had ceased. The temperature was reduced to 1650°C, at a rate of 50°C per minute, where pressure was released and then furnace power was shut off and the furnace was allowed to cool to room temperature. Hot pressed billets were all approximately 5 mm thick. After hot-pressing, the resulting billets were ground flat and parallel using a manual surface grinder (FSG-618, Chevalier, Santa Fe Springs, CA) to roughly 4.2 mm thick using a 120-grit diamond wheel. Two ground rectangular billets of each composition were each sectioned into three 12 mm x 31 mm coupons and one 10.5 mm x 31 mm coupon via electrical discharge machining (HSS-150, Agie, Lincolnshire, IL). A modified Archimedes method using distilled water was employed to measure the bulk densities of each composition prior to welding (ASTM C373). Coupons were boiled for 2 hours and then held under vacuum for 15 minutes. Theoretical densities for the batched compositions were based on a rule-of-mixtures calculation assuming the theoretical densities of 3.21 g/cm³ for SiC, 6.09 g/cm³ for ZrB₂, and 6.63 g/cm³ for ZrC.^{22,23}

2.2 Welding, Arc Melting, and Melting Temperature

The two smallest coupons from each billet were cut into thirds on the Chevalier surface grinder with a resin-bonded diamond cutting wheel to produce sacrificial starting/ending pieces for welds. Two specimens and two of the sacrificial pieces were arranged on a graphite setter as shown in Figure 2. The setter and components were then bonded with cyanoacrylate adhesive to prevent movement and placed inside a glove box (MBraun, UL04-178, Garching, Germany). The glovebox was maintained under an argon atmosphere and the setter was placed onto a graphite heating plate. The setter was covered with graphite felt insulation, and preheated at 10°C per minute to 1450°C. Temperature was measured using B-type thermocouple placed near the setter under the graphite felt. Using a linear tracker with a Tungsten Inert Gas (TIG) welding torch attached to it, straight fusion welds were made on the preheated specimen

assemblies inside the glove box. The fusion welds were produced using the lift TIG method with an argon flow of 35 SCFH through the torch and a travel speed of 14 cm/min on the linear tracker. Each composition was joined using welding currents of 160, 180, and 200 amps. After welding, the specimen assembly was covered with graphite felt and allowed to equilibrate to 1450°C. It was then cooled at 10°C per minute to 1350°C, held for one hour to anneal, and cooled at 5°C per minute to room temperature. Once cooled, welded specimens were removed from the glovebox and cross sectioned at various points in the weld to investigate weld width, penetration depth (defined as the distance that liquid infiltrates into the 4.2 mm thick specimens, measured downwards from the top of the coupons), and overall liquid formation to evaluate weldability. The cross-sectioned specimens were mounted into an epoxy resin and polished to a 0.25 µm diamond finish. After polishing, the sections were viewed under an optical microscope (KH-8700, HIROX-USA, Inc., Hackensack, NJ) to study microstructures.

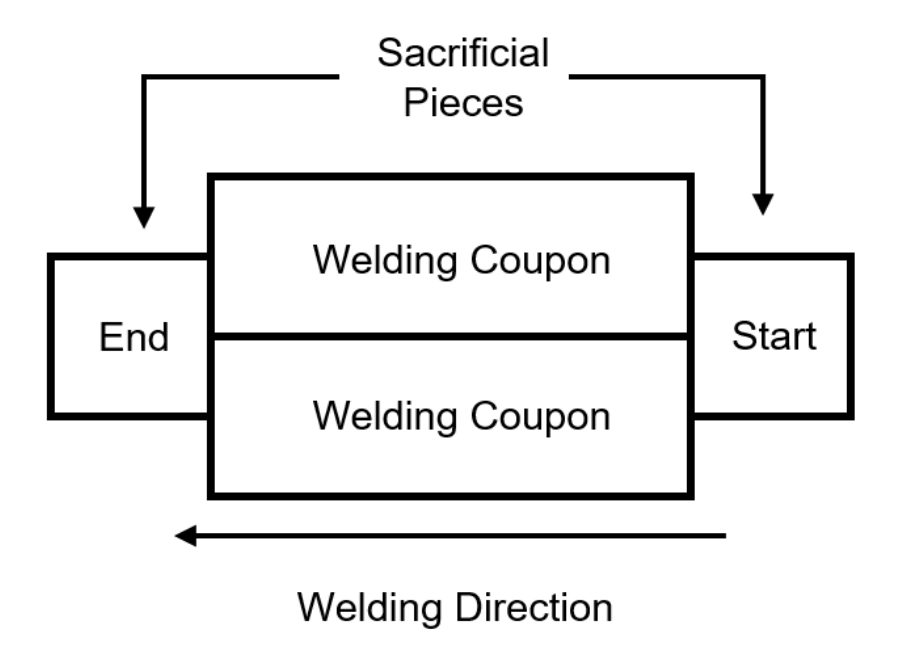


Figure 2: Schematic of the coupon arrangement for welding. Welding coupons were 31 mm by 12 mm and sacrificial start and end pieces were 9 mm by 14 mm.

Additional powder mixtures in the SiC, ZrB₂, ZrC binaries were batched for arc melting to determine compositions of the eutectics in the binary phase systems that made up the SiC-ZrB₂-ZrC

ternary system. Binary joins were drawn from the binary eutectics to the ternary eutectic as a first approximation of boundary line locations between primary crystallization fields. Three compositions along each join were batched and arc melted to determine the location of the boundaries between phase fields in the ternary phase diagram. All binary and ternary powder compositions for arc melting were batched without sintering aids. Powders were ball mixed for two hours in acetone with SiC media.

Powder was dried via rotary evaporation, ground through a 200-mesh sieve and pressed into pellets that were roughly 1.3 cm diameter by 1 cm tall. Pressed pellets were then arc melted in an argon environmental chamber with a Miller Intelliweld power supply and a tungsten electrode on a water-cooled copper hearth. Current was slowly increased through the pellets until all powders formed a continuous bead of liquid. After melting two times, the melted samples were cross-sectioned, mounted in epoxy resin, and polished to a 0.25 µm finish.

Melting temperature experiments were performed on the ternary eutectic composition described by R. Tu et al. and the SiC-ZrB₂ binary eutectic composition reported by H. Tu et al. using a resistance-heated graphite element furnace (3060-FP20, Thermal Technology, Santa Rosa, CA).^{19, 24} The furnace was setup so that a portion of a hot pressed billet could be observed through a shaded lens while at temperature. Temperature was ramped at 50°C/min up to 2000°C and then increased at 10°C/min to 2200°C and then at 1°C/min until melting was observed visually.

2.3 Characterization

Microstructure analysis was performed using a scanning electron microscope (SEM; TM-1000, Hitachi, Krefeld, Germany). Micrographs were processed using the BlueQuartz software package (BlueQuartz, Springboro, Ohio) which segmented each phase into a specific color. The processed image could then be imported into ImageJ (Rasband, W.S, U. S. National Institutes of Health, Bethesda, MD) to measure the area percent (area%) of each phase. The microstructure was assumed to be homogeneous and isotropic allowing the measured area% to be converted directly into vol%. These vol% were used to plot the compositions of the phase boundaries across the ternary phase diagram for the system. ImageJ was

also used to determine the grain size of SiC from micrographs taken of hot-pressed billets before welding was performed. At least 400 grains were measured from each composition.

X-ray Diffraction (XRD) was performed on machined parent material coupons and fusion zones of welded samples to establish the phases present after hot pressing and welding, respectively. Welded specimens were polished in a top-down fashion into the weld surface and scanned with a PANalytical X'Pert diffractometer (Malvern PANalytical Ltd., Royston, United Kingdom). Cu-Kα radiation was used as the x-ray source. Accelerating voltage was set to 45 keV and the filament current was set to 45 mA. Scans used a step size that would complete each run in approximately 30 minutes for a range of 0-90° 2θ. Patterns were analyzed using an automatic Hanawalt "search and match" method in the X'Pert Highscore software (version 2.2e) to find the best match material. Search parameters used a minimum significance value of 3, a minimum and maximum tip width of 0.10 and 1.0 respectively, and a peak base width of 2.0 in the "Search 3" mode.

Raman spectroscopy was performed on several polished specimens to determine if free carbon was present. Measurements were collected using a HORIBA Jobin Yvon LabRAM ARAMIS microRaman spectrometer (Horiba, Edison, NJ). A 632 nm He/Ne laser was used to excite polished specimens and was focused to a 2 to 3µm spot size using a 50x microscope objective lens. Laser power was kept below 2 mW to prevent local heating. Three spectra were taken on each inspected sample, with all measurements conducted at room temperature

Carbon analysis (CS600; Leco, St. Joseph, MI) was performed on sub 200-mesh ground powders of commercially available ZrC powder from Table 1, hot pressed ZrC (without sintering aids), and hot pressed and arc melted ZrC. Three empty baseline tests were run then three standards were run (WC #501-123, 6.23±0.04 C, LECO, St. Joseph, MI) to calibrate the machine before testing three samples of each powder.

3. Results and Discussion

3.1 XRD, Densities, and Microstructures of Parent Materials

A series of SiC-ZrB₂-ZrC ceramic compositions were produced for welding studies. The compositions were spaced along a binary join between pure SiC and the ternary eutectic area determined by King et al. in an attempt to achieve primary crystallization of SiC followed by crystallization of only the ternary eutectic. ¹⁶ XRD scans performed on the parent material of each tested composition showed that only SiC, ZrB₂, and ZrC were present after hot-pressing. A representative secondary electron image of the parent materials observed in the study (with phases identified) can be seen in Figure 3. Further information on all compositions batched on the binary join in the current study, including their bulk density, theoretical density, and SiC grain size in the parent material can be found in Table 2.

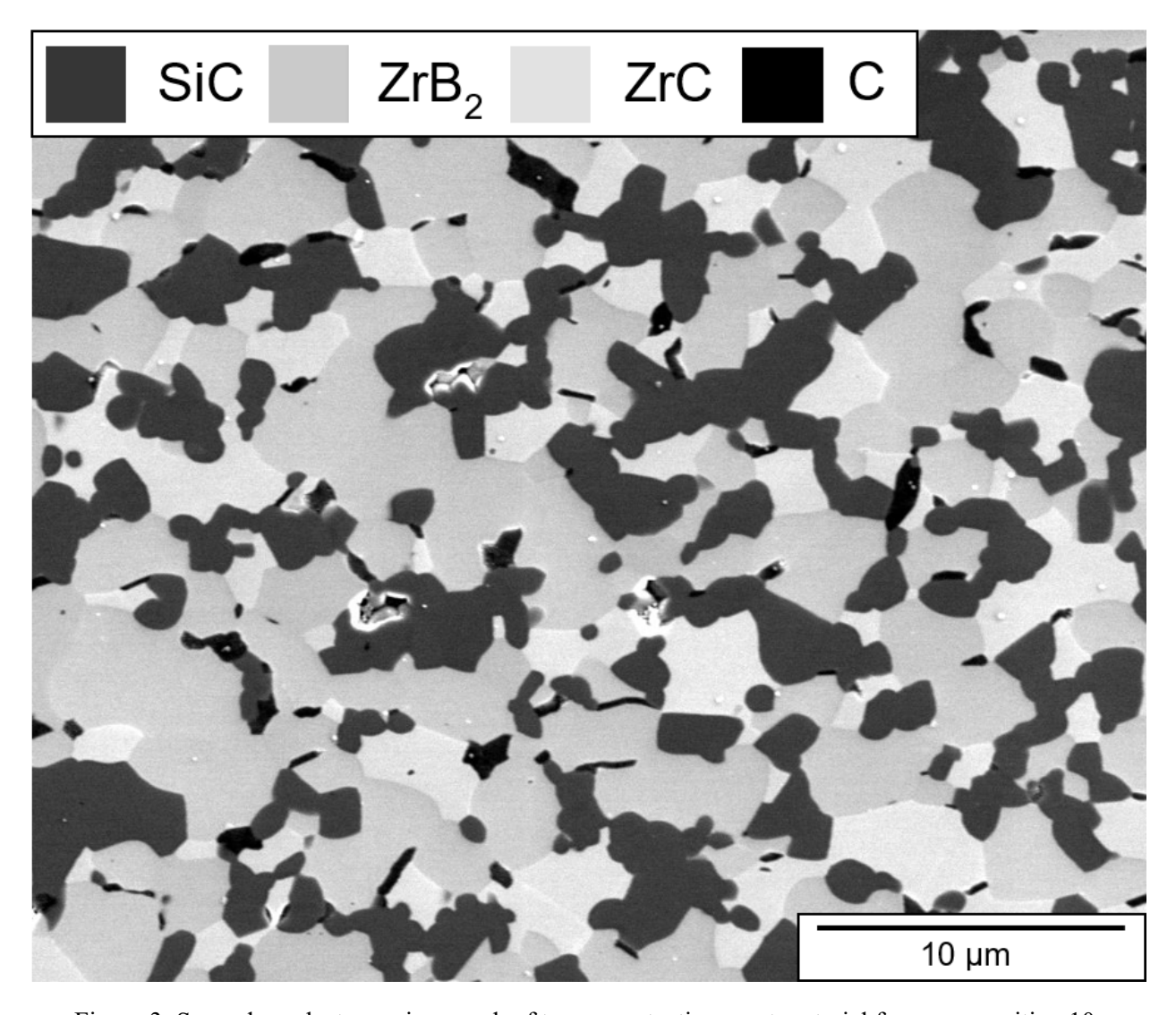


Figure 3: Secondary electron micrograph of ternary eutectic parent material from composition 10.

3.2 Weld formation of SiC-ZrB₂-ZrC composites as a function of SiC

TIG welds performed on the various compositions determined from the binary join, seen in Figure 1, showed a range of weldability. Weldability was qualitatively assessed based on the amount/size of porosity between the parent material and the fusion zone, fluid retention within the fusion zone, and the flow behavior of the composition that was observed during welding.

A representative secondary electron image of the microstructure of a successfully welded composition is shown in Figure 4. Welded microstructures were comprised of large primary SiC grains

and solidified eutectic composed of fine lamella that formed on cooling. An inset image was also included in Figure 4 to reveal the difference in contrast between ZrB₂ and ZrC in the welded fusion zones.

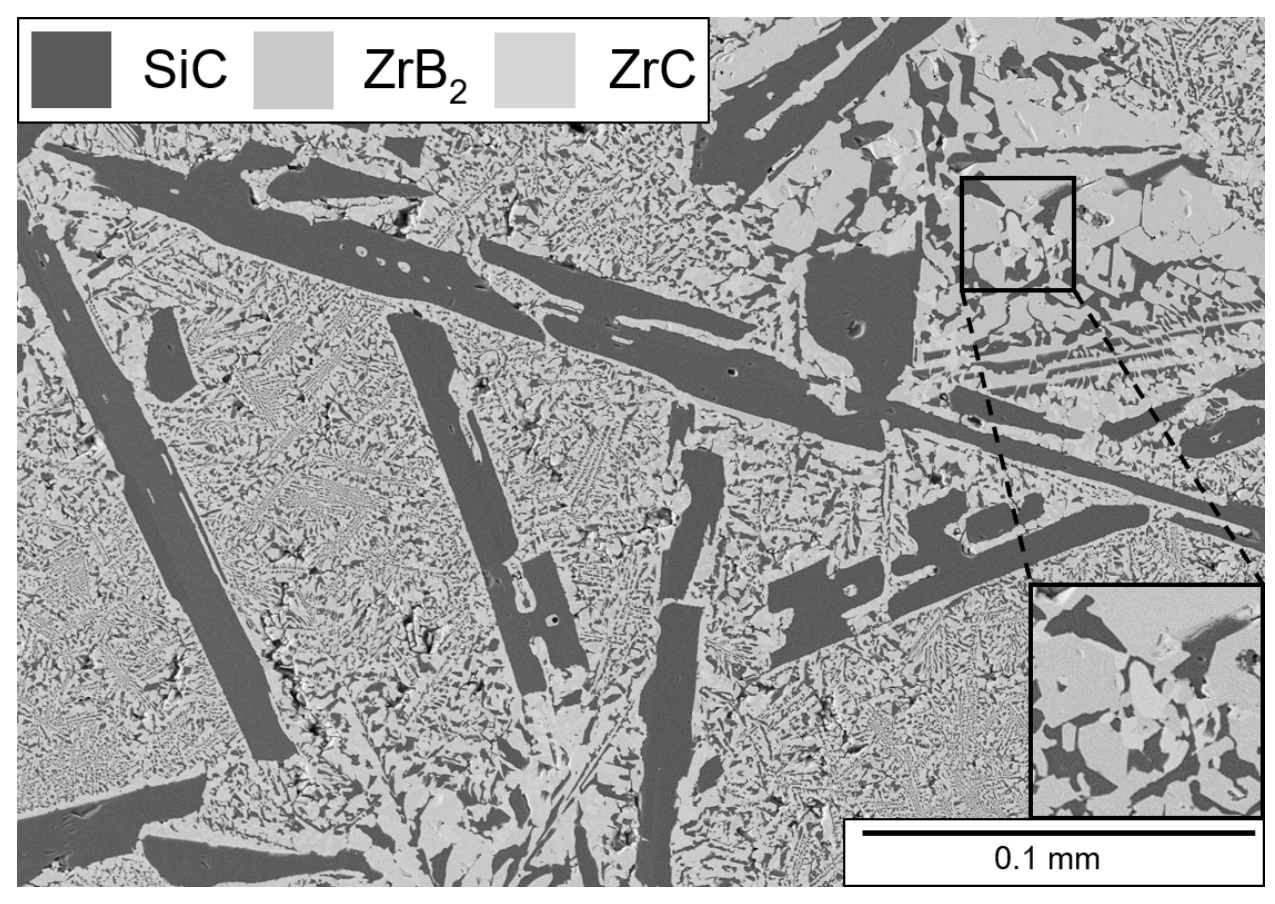


Figure 4: Secondary electron micrograph of welded microstructure from composition 7. The inset image contains all three phases to highlight the slight contrast difference between ZrB₂ and ZrC.

Compositions above ~63 vol% SiC content were not weldable. When joining was attempted using composition 1, a gaseous reaction product was produced and only a small amount of liquid formed, which joined the coupons during the 200 A weld. SEM image analysis on the solidified liquid region showed that its composition was roughly 65 vol% SiC, 17.5 vol% ZrB₂, and 17.5 vol% ZrC compared to its initial composition of 74.3 vol% SiC, 15.9 vol% ZrB₂, and 9.8 vol% ZrC. Presumably, SiC was lost as the gaseous product observed during welding. Based on gas formation during joining attempts, 65 vol% SiC appears to be the maximum SiC content that can be welded since liquid did not form during welding until gas formation reduced the SiC content to that amount. Compositions 2 and 3 were then tested to

determine if batches above and below 65 SiC (vol%) on the binary join would form liquid during welding. Composition 2 showed gas formation during all attempted welds with no liquid formation. This was expected since its initial SiC content was 68.5 vol%. All three welds performed on composition 3 formed liquid without gas formation and produced a fusion zone. The liquid that formed appeared very viscous and was partially blown out of the fusion zone. This left large "valleys" in all of the welds attempted on composition 3 along with large pores, likely from gasses that were trapped in the viscous liquid. Composition 3 did show successful joining; however, this composition was not considered to be weldable based on the liquid removal and sizes of the pores (Figure 5). Composition 4 was ZrC-rich compared to the binary join, but with a similar SiC content to composition 3 to determine if increasing the ZrC content would promote weldability. This weld exhibited problems with wetting during liquid formation. Droplets of SiC-ZrC rich liquid formed on the coupon surface instead of penetrating the joint, which resulted in poorly joined samples. Hence, compositions 1-4 did not form workable welds due to gas formation, viscous liquids, and poor wetting behavior.

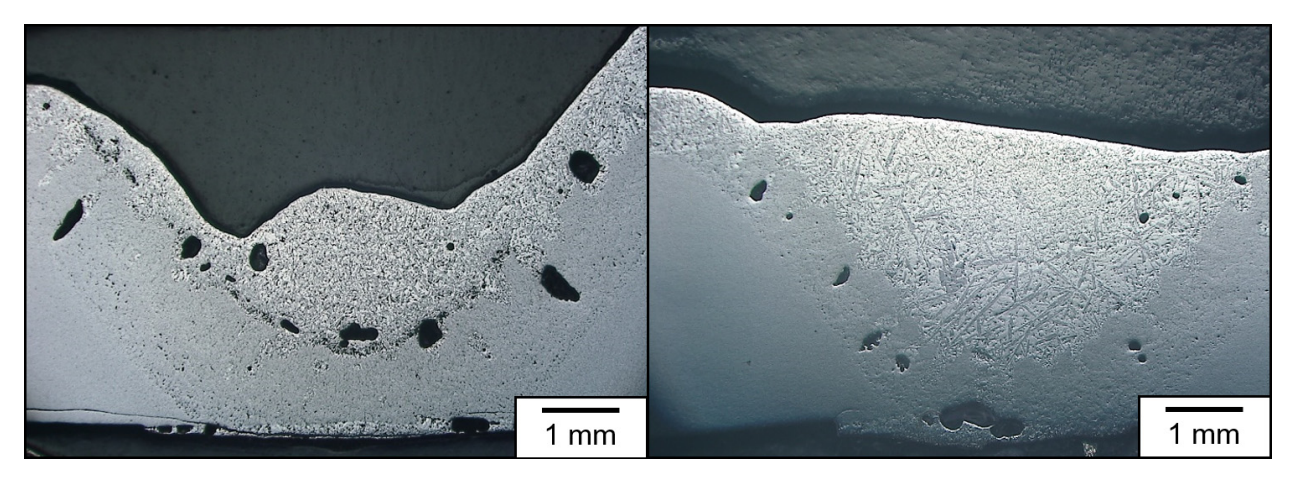


Figure 5: Optical micrographs of the cross sections of welds from composition 3 (left) and composition 5 (right).

Compositions containing less than ~63 vol% SiC were found to be weldable. Welds performed on samples starting with composition 5 showed better penetration depth, fluid retention, and a decrease in the size of pores. Composition 5, which contained 57.3 vol% SiC, was determined to be the upper limit for

SiC content on the binary join that could be welded. While large pores were observed between the fusion zone and the parent material, the fluid remained in the weld and joined the coupons (Figure 5). The largest grains of SiC observed in the cross sections of these welds were 1 to 1.5 mm long. As SiC content decreased on the binary join from composition 5 towards composition 8, liquids formed during welding appeared less viscous, remained within the weld area, and produced increasingly better welds with little to no porosity. A large range of microstructures and grain sizes of SiC were observed for these compositions as seen in Figure 6. Composition 6 (52 vol% SiC) produced the largest SiC grains of any composition in the current study, which were up to ~1.5 to 2 mm long. In compositions 7 and 8, SiC grain size dropped rapidly to produce grains that were up to ~450 μm and ~225 μm, respectively. This drastic decrease in grain size occurred as the SiC content of the compositions decreased along the binary join. When compositions were located further away from a phase field boundary (i.e., higher SiC content), the primary crystals grew across a wider range of temperatures (i.e., the difference between the liquidus and solidus temperatures was greater), which produced larger grains. As compositions shifted toward the ternary eutectic, the liquidus temperature decreased, which resulted in less time for the primary crystals to grow and produced smaller overall SiC grains. The increase in grain size from composition 5 to 6 is attributed to SiC content in the welds. In composition 5, more SiC was present meaning more initial SiC primary crystallites formed. As these grew during cooling, the crystallites impinged upon each other and impeded grain growth. The lower SiC content in composition 6 produced a more open microstructure with fewer initial primary crystallites. With fewer crystallites, more room was present to allow grains to grow unimpeded. Compositions containing less than ~63 vol% SiC were shown to have controllable microstructures when fusion welded as compositions moved further away from the ternary eutectic.

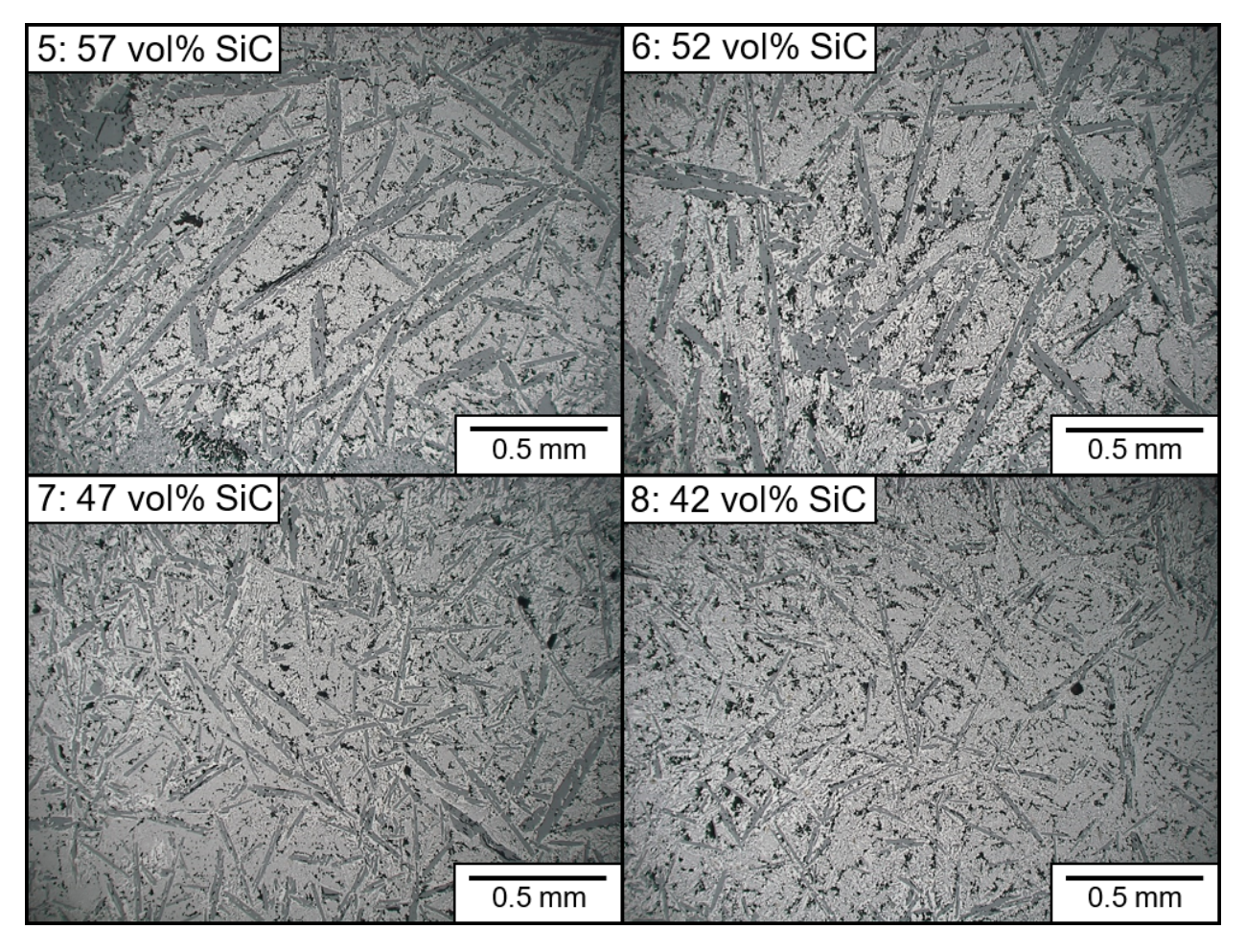


Figure 6: Optical micrographs showing microstructures of fusion zones from welds of compositions 5-8.

Decreasing the SiC content also affected the formation of free carbon during the solidification of the melt pool. As SiC content decreased below 57 vol% towards composition 9, increased amounts of free carbon were observed in the fusion zones. The free carbon that was observed in the fusion zones of compositions 5 to 9 is presumed to have been produced by the formation of carbon vacancies in ZrC. To support this hypothesis, the carbon contents of commercial ZrC powder, a hot-pressed ZrC billet, and arc melted ZrC hot-pressed billets were tested in a carbon analyzer. The as-received powder was determined to have a composition of ZrC_{0.92}, hot-pressed material was ZrC_{0.95}, and arc melted material was ZrC_{0.72}. The drastic decrease in carbon content of the arc melted material suggests that carbon could be released into the melt when ZrC forms a liquid during welding.²⁵

The presumed ternary eutectic, composition 9, was successfully welded, but still showed evidence of primary SiC crystallization and secondary crystallization of SiC-ZrC binary eutectic, as seen in Figure 7. This indicated that the actual composition of the eutectic was different than the composition determined by King et al. Image analysis of high contrast SEM images of multiple ternary eutectic areas from different welds identified the ternary eutectic composition as 36.9±1.3 vol% SiC, 42.7±1.5 vol% ZrB₂, and 20.4±1.9 vol% ZrC. This composition was, within variance, the same as the ternary eutectic composition recently proposed by R. Tu et al. Image 19, and was batched as composition 10.

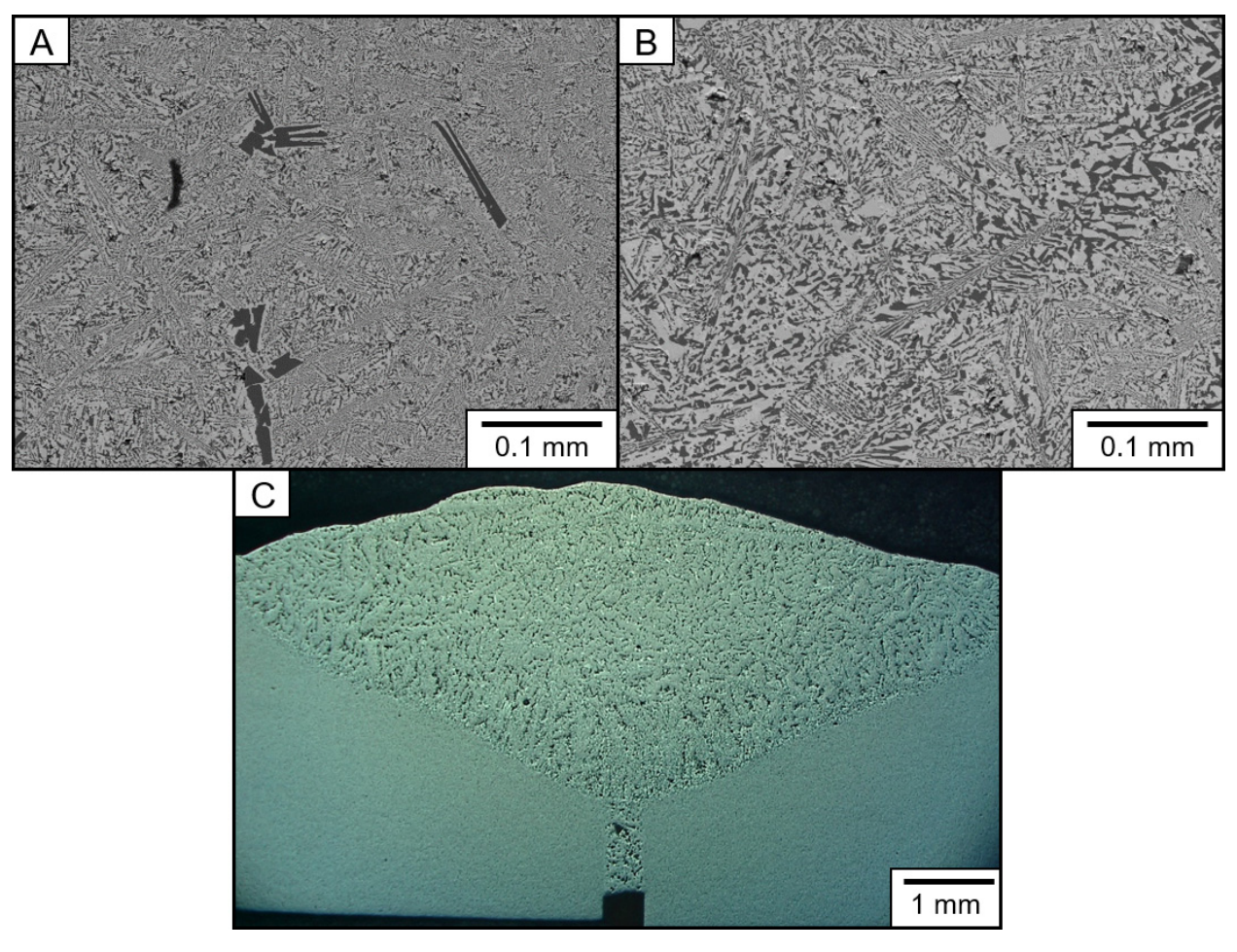


Figure 7: SEM micrographs showing microstructures of fusion zones from welds of compositions 9 (A), composition 10 (B), and the entire fusion zone of composition 10 (C).

Microstructural analysis of welds of composition 10 revealed a much more uniform microstructure comprised of almost entirely eutectic lamella and free carbon as seen in Figure 7.

Composition 10 showed the best weldability of any compositions tested with no porosity, low viscosity melts, and retention of the fluid in the joint during welding. Although microstructure control was possible away from the ternary eutectic on the binary join, compositions closer to the eutectic showed the best penetration depth, fluid retention, and little to no porosity.

The penetration depth of welds into the 4.2 mm thick coupons correlated to the welding amperage for compositions 5 to 10. For example, welds performed at 160A showed 60 to 70% penetration, 180A welds showed 70 to 80% penetration, and the maximum current of 200A showed 100% penetration of the 4.2 mm thick coupons. Penetration depth of the coupons was also affected by the speed at which the welding torch was translated. A translation rate of 14 cm/min provided the best results. Slower travel speeds resulted in the weld torch cutting into the coupons due to the larger heat input, while faster travel speeds provided lower heat input into the coupons causing less penetration since the coupons had less time to melt and join. Based on these results, depth penetration of weldable compositions was controllable by changing both the travel speed of the linear tracker and the current input to the TIG torch.

3.3 The SiC-ZrB₂-ZrC ternary phase diagram

Investigated compositions used to construct a ternary phase diagram for the SiC-ZrB₂-ZrC system were melted and image analysis was performed on the resulting microstructures. To validate the underlying assumption that the compositions determined from image analysis (i.e., area percents in images) were equivalent to the volume percentages used to batch the compositions and construct the diagram, sections were cut from hot pressed billets that were orthogonal to each other. The orthogonal sections were examined for each of the binary eutectic compositions and the ternary eutectic composition to determine if compositions estimated from image analysis were affected by the orientation. Hot-pressed billets were then are melted, sectioned a second time on orthogonal faces, polished, and analyzed. For both the hot pressed and are melted materials, the area fractions measured on the orthogonal faces were all consistent with the batched compositions, which indicated that image analysis of cross sections provided a reasonable estimate of composition.

As a first step in producing a revised SiC-ZrB₂-ZrC phase diagram, each of the three binary systems was investigated to determine the binary eutectic compositions. In the SiC-ZrB₂ system, Ordan'yan reported a binary eutectic composition of 69.3 vol% SiC and 30.7 vol% ZrB₂.²⁶ Little information was reported on how this diagram was constructed, or the purity of starting materials, but a recent study used electron microprobe analysis to identify a binary eutectic composition of 48.7 vol% SiC and 51.3 vol% ZrB₂.²⁴ In the present study, the latter composition was melted and the composition of the SiC-ZrB₂ binary eutectic was determined to be 48.1±1.9 vol% SiC and 51.9±1.9 vol% ZrB₂ from image analysis. With such a close agreement, the microprobe results were used for the location of the SiC-ZrB₂ binary eutectic.

In the ZrB₂-ZrC system, previous reports showed a range of binary eutectic compositions from 38 vol% to 48 vol% ZrC, which varied with the carbon stoichiometry of ZrC.^{27–29} As a starting point, a composition of 43.5 vol% ZrC was arc melted. Analysis of the ZrB₂-ZrC eutectic microstructure showed a composition of 52.4±2.1 vol% ZrB₂ and 47.6±2.1 vol% ZrC. This composition was selected as the location of the ZrB₂-ZrC binary eutectic and suggests that ZrC had a carbon concentration of ZrC_{0.9}, based on the analysis of Sorrell et al.³⁰

Few studies have examined the SiC-ZrC binary phase diagram. Hence, pellets of SiC and ZrC powders with a range of compositions over the entire binary system were made, arc melted, sectioned, and polished. A composition of 64 vol% SiC and 36 vol% ZrC was the easiest to melt, suggesting that it may be near the eutectic composition; however, eutectic microstructures were not observed, and gas formation occurred during melting. Brukl previously determined that the composition with the lowest melting temperature in the system was 44.5 vol% SiC and 55.5 vol% ZrC.³¹ Since the SiC-ZrC eutectic was unknown, both compositions were batched as possible binary eutectic locations. Gas formation occurred when melting both compositions, indicating partial decomposition of the SiC. No regions of eutectic microstructure were found for these materials. As a result, both compositions were kept as possible SiC-ZrC binary eutectic locations.

The binary eutectic compositions identified above for SiC-ZrB₂, ZrB₂-ZrC, and SiC-ZrC and the ternary eutectic discussed previously were plotted on a ternary phase diagram in Figure 8. Binary joins were added between each binary eutectic and the ternary eutectic. Various specimens were created with compositions across each of the binary joins. For all the compositions on the joins between the ternary eutectic and the SiC-ZrB2 and ZrB2-ZrC binary eutectics, ZrB2 was the primary crystal to form. In contrast, SiC was the primary crystal to form for compositions on the joins between the ternary eutectic and the possible SiC-ZrC binary eutectic locations. The amounts of primary crystallization that formed in the binary join samples were measured from SEM micrographs using image analysis to estimate the location and inflection of the phase field boundaries using the inverse ternary lever rule, as seen in Figure 8. Compositions with the lowest amount of ZrB2 on both SiC-ZrC binary joins could not be analyzed because gas formation occurred during melting and changed their composition. Without these samples or a binary eutectic location, the boundary line connecting to the SiC-ZrC binary could not be completed. The portion of the boundary line that was determined was highly curved, which produced a narrow range of weldable compositions that form ZrC as a primary phase followed by ternary eutectic crystallization. Fortunately, this is the only phase field in the system with such a restriction. In general, the proposed diagram in Figure 8 will change with the carbon stoichiometry of ZrC. As ZrC stoichiometry changes, the compositions of the associated binary eutectics will change, which will affect the curvature of the phase field boundary lines.

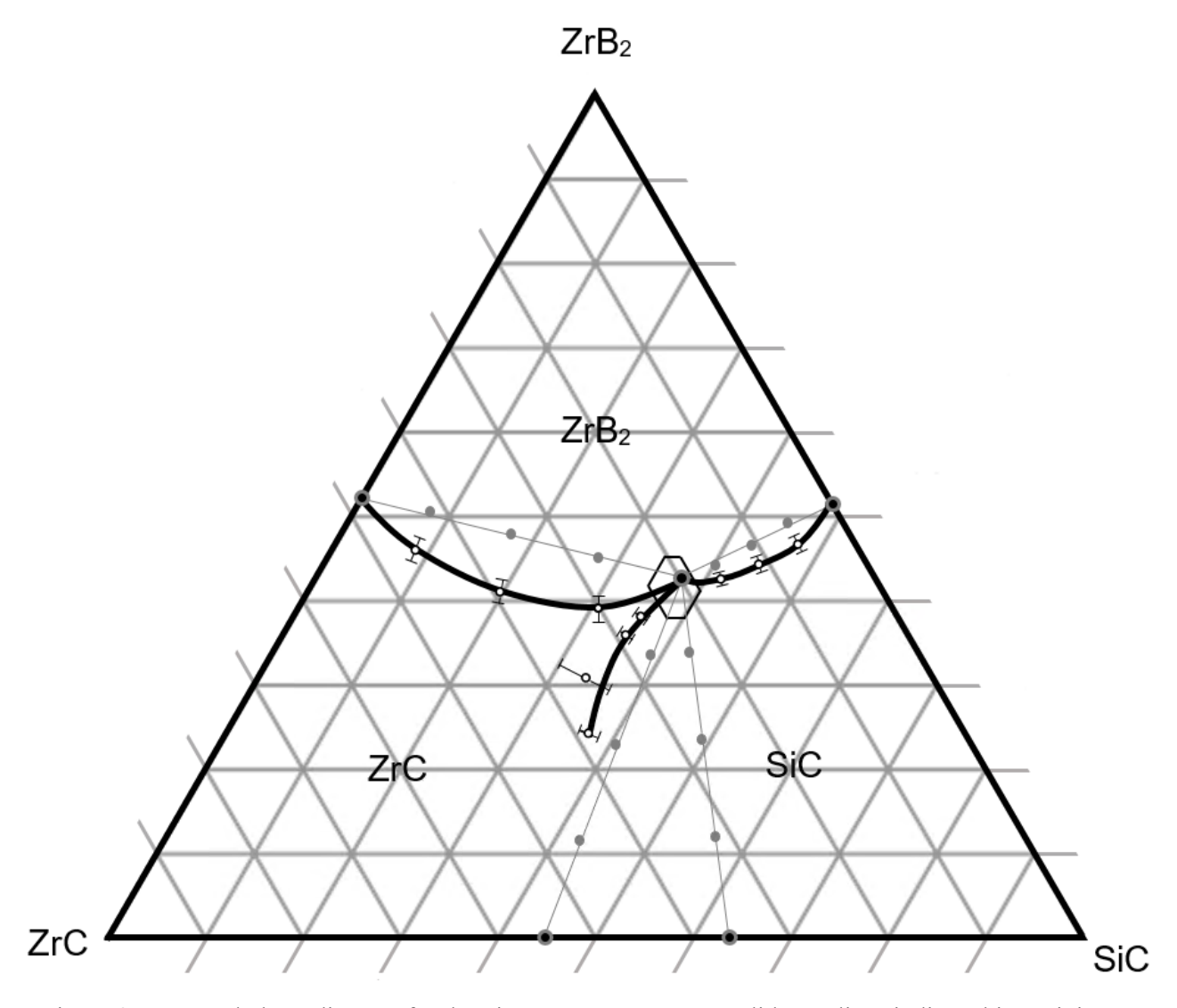


Figure 8: Proposed phase diagram for the SiC-ZrB₂-ZrC system. Solid grey lines indicate binary joins, solid grey circles indicate the tested compositions on the join, hollow black circles indicate the phase field boundary locations and their associated deviation measured, and solid black lines represent the overall phase field boundaries.

The results from the present study suggest that a minimum amount of ZrB₂ is necessary to enable liquid formation during arc melting and prevent dissociation of SiC. Both of the last SiC-ZrC binary join compositions, the SiC-ZrC binary eutectic estimations, and compositions 1, 2, and 4 from the weldability study contained less than 20 vol% ZrB₂ and were unable to be joined and/or melted due to poor wettability and poor liquid formation. The liquid formed by composition 1 contained 65 vol% SiC, 17.5 vol% ZrB₂, and 17.5 vol% ZrC, which suggests that 17.5 ZrB₂ vol% may be the lower limit of ZrB₂

content for welding. However, Composition 2 challenged this hypothesis since it contained 19 vol% ZrB₂, but did not form any liquid during welding. Since only a small area of liquid formed when composition 1 was melted, the estimated liquid composition may not be accurate. For this reason, the lower bound for ZrB₂ required to weld was set at ~20 vol% ZrB₂. While Composition 4 did form liquid despite having a ZrB₂ content of only 14.8 vol%, the liquid that formed was rich in ZrC and non-wetting, which suggested that more ZrB₂ was required. No upper bound for the ZrB₂ required for welding was determined. All of the compositions that contained more than 20 vol% ZrB₂ in the current study formed appreciable amounts of liquid and exhibited wetting behavior. Further, previous research studies for welding in the ZrB₂-SiC and ZrB₂-ZrC systems indicated compositions containing more than 60 vol% ZrB₂ were weldable. ^{15, 32}

Melting temperature experiments performed on the proposed ternary eutectic (composition 10) showed that the onset of melting was coincident with total melting at 2330±23°C. The melting point measured in the present study for composition 10 was higher than the value reported by R. Tu et al. by $\sim 50^{\circ}$ C. ¹⁹ The pyrometer used in the present study has a precision of $\pm 1\%$. Although no precision was reported for the temperature measurements by R. Tu, a similar precision would make these temperatures nominally identical given the overlap of the variances in the two measurements. In an effort to further substantiate the temperature measured by the pyrometer in the present study near the melting temperature of the ternary eutectic, a pure alumina pellet was pressed from high-purity powders (99.9% purity, NanoTek alumina, Nanophase Technologies Co., Romeoville, IL) and melted. The alumina pellet was observed to melt at 2060°C and compared to the melting point reported by Klug of 2054±6°C.33 Therefore, the pyrometer appears to have high precision in the temperature range of interest. For the SiC-ZrB₂ binary eutectic composition, the onset of melting occurred at 2340±23°C and total melting occurred at 2360±23°C. Differing onset and total melting values for the binary eutectic composition indicated that the batched composition deviated from the actual eutectic composition, although only slightly. The onset of melting from the present study was higher than binary eutectic temperatures of 2270±30°C from Ordan'yan and 2297°C from H. Tu. 24,26 . The precision of the pyrometer ($\pm 1\%$) can account for most of

the difference between reported values and the present study, but powder purity may also play a role in the differences.

4. Conclusion

The fusion welding of SiC-ZrB₂-ZrC compositions was studied. Dense ceramics were preheated and welded at amperages from 160 to 200 A. Penetration was shown to be tailorable both by welding amperage and travel speed with welds performed at 200 A showing full penetration in the 4.2 mm thick coupons for weldable compositions. The compositions that were weldable contained ~36 vol% to 57.5 vol% SiC and were on a binary join between the ternary eutectic composition and pure SiC. The size of primary SiC grains in the fusion zones could be controlled by the overall composition. The ternary eutectic was the best overall composition for welding. A ternary phase diagram was proposed for SiC-ZrB₂-ZrC system with a ternary eutectic temperature of 2330±23°C and a composition of 36.9±1.3 vol% SiC, 42.7±1.5 vol% ZrB₂, and 20.4±1.9 vol% ZrC. Analysis of microstructures of are melted compositions were used to add boundary lines between primary crystallization fields, but the boundary line between the ternary eutectic and the ZrC-SiC binary eutectic could not be completed due to the low content of ZrB₂, which resulted in gas formation during melting. Overall, a minimum ZrB₂ content of 20 vol% is needed for welding of SiC-ZrB₂-ZrC ceramics, based on liquid wetting behavior and formation of gaseous species during melting.

5. Acknowledgement

This work was funded by a Department of Energy phase II SBIR (DE-SC0017082) through a subcontract from UES Inc. contract #0055606 U.S.

References:

- Katoh Y, Snead LL, Henager CH, et al. Current status and critical issues for development of SiC composites for fusion applications. J Nucl Mater. 2007;367-370 A(SPEC. ISS.):659–671. https://doi.org/10.1016/j.jnucmat.2007.03.032
- 2. Price RJ. Properties of silicon carbide for nuclear fuel particle coatings. *Nucl Technol*. 1977;35(2):320–336. https://doi.org/10.13182/NT77-A31892
- 3. Ray D, Flinders M, Anderson A, Cutler RA RW. Effect of room-temperature hardness and toughness on the ballistic performance of SiC-based ceramics. *Adv Ceram Armor*. 2005;131–142.
- Hou Z, Luo R, Yang W, Xu H, Han T. Effect of fiber directionality on the static and dynamic mechanical properties of 3D SiCf/SiC composites. *Mater Sci Eng A*. 2016;658:263–271. https://doi.org/10.1016/j.msea.2016.02.006
- Xu Y, Cheng L, Zhang L, Yin H, Yin X. High toughness, 3D textile, SiC/SiC composites by chemical vapor infiltration. *Mater Sci Eng A*. 2001;318(1–2):183–188.
 https://doi.org/10.1016/S0921-5093(01)01303-X
- 6. Droillard C, Lamon J. Fracture toughness of 2-D woven SiC/SiC CVI-composites with multilayered interphases. *J Am Ceram Soc.* 1996;79(4):849–858. https://doi.org/10.1111/j.1151-2916.1996.tb08516.x
- Zhuang Li, Asish Ghosh, Albert S. Kobayashi and RCB. Indentation Fracture Toughness of Sintered Silicon Carbide in the Palmqvist Crack Regime. *J Am Ceram Soc.* 1989;72(6):904–911. https://doi.org/10.1111/j.1151-2916.1991.tb06949.x
- Zinkle SJ. Advanced irradiation-resistant materials for Generation IV nuclear reactors. Elsevier
 Ltd; 2017 https://doi.org/10.1016/B978-0-08-100906-2.00016-1
- Zinkle SJ, Was GS. Materials challenges in nuclear energy. *Acta Mater*. 2013;61(3):735–758.
 https://doi.org/10.1016/j.actamat.2012.11.004
- 10. Snead LL, Nozawa T, Ferraris M, Katoh Y, Shinavski R, Sawan M. Silicon carbide composites as fusion power reactor structural materials. *J Nucl Mater*. 2011;417(1–3):330–339.

- https://doi.org/10.1016/j.jnucmat.2011.03.005
- 11. Singh M, Matsunaga T, Lin HT, Asthana R, Ishikawa T. Microstructure and mechanical properties of joints in sintered SiC fiber-bonded ceramics brazed with Ag-Cu-Ti alloy. *Mater Sci Eng A*. 2012;557:69–76. https://doi.org/10.1016/j.msea.2012.05.110
- 12. Nguyen LM, Leguillon D, Gillia O, Riviere E. Bond failure of a SiC/SiC brazed assembly. *Mech Mater*. 2012;50:1–8. https://doi.org/10.1016/j.mechmat.2012.03.001
- 13. Rice R. Advances in Joining of Ceramics. *Adv. Join. Technol. proceeding 4th army Mater.*Technol. Conf. 1976:69–111. https://doi.org/10.1002/9781118405802
- 14. Ruff O. The Formation and Dissociation of Silicon Carbide. *Trans Electrochem Soc.* 1935;68(1):87. https://doi.org/10.1149/1.3493894
- Hilmas G, Fahrenholtz W, Watts JL, Brown-Shaklee HJ. Ceramic Welds, and a Method for Producing the Same. US 8,715,803 B2. 2014.
- King DS, Watts JL, Cissel KS, Kadhim AH, Hilmas GE, Fahrenholtz WG. Solidification of welded SiC–ZrB2–ZrC ceramics. *J Am Ceram Soc*. 2018;101(9):4331–4339. https://doi.org/10.1111/jace.15570
- 17. Akin I, Goller G. Mechanical and oxidation behavior of spark plasma sintered ZrB 2-ZrC-SiC composites. *J Ceram Soc Japan*. 2012;120(1400):143–149. https://doi.org/10.2109/jcersj2.120.143
- Guo SQ, Kagawa Y, Nishimura T, Chung D, Yang JM. Mechanical and physical behavior of spark plasma sintered ZrC-ZrB2-SiC composites. *J Eur Ceram Soc.* 2008;28(6):1279–1285. https://doi.org/10.1016/j.jeurceramsoc.2007.08.009
- 19. Tu R, Xiao B, Zhang S, et al. Mechanical, electrical and thermal properties of ZrC-ZrB2-SiC ternary eutectic composites prepared by arc melting. J Eur Ceram Soc. 2018;38(11):3759–3766. https://doi.org/10.1016/j.jeurceramsoc.2018.04.028
- 20. Zhu S, Fahrenholtz WG, Hilmas GE, Zhang SC. Pressureless sintering of zirconium diboride using boron carbide and carbon additions. *J Am Ceram Soc.* 2007;90(11):3660–3663. https://doi.org/10.1111/j.1551-2916.2007.01936.x

- Zhang SC, Hilmas GE, Fahrenholtz WG. Pressureless densification of zirconium diboride with boron carbide additions. *J Am Ceram Soc.* 2006;89(5):1544–1550. https://doi.org/10.1111/j.1551-2916.2006.00949.x
- 22. Wu WW, Zhang GJ, Kan YM, Wang PL. Reactive hot pressing of ZrB2-SiC-ZrC composites at 1600°C. *J Am Ceram Soc.* 2008;91(8):2501–2508. https://doi.org/10.1111/j.1551-2916.2008.02507.x
- 23. Gasparrini C, Rana D sham, Le Brun N, *et al.* On the stoichiometry of zirconium carbide. *Sci Rep.* 2020;10(1):1–12. https://doi.org/10.1038/s41598-020-63037-0
- 24. Tu H, Hirayama H, Goto T. Preparation of ZrB2-SiC composites by arc melting and their properties. *J Ceram Soc Japan*. 2008;116(1351):431–435. https://doi.org/10.2109/jcersj2.116.431
- 25. Jackson HF, Jayaseelan DD, Manara D, Casoni CP, Lee WE. Laser melting of zirconium carbide: Determination of phase transitions in refractory ceramic systems. *J Am Ceram Soc*. 2011;94(10):3561–3569. https://doi.org/10.1111/j.1551-2916.2011.04560.x
- Ordan'yan S, Dmitriev I, Moroshkina E. Reaction of SiC with ZrB2. Neorg Mater.
 1989;25(10):1752–1754.
- 27. Goutier F, Trolliard G, Valette S, Maître A, Estournes C. Role of impurities on the spark plasma sintering of ZrCx-ZrB2 composites. *J Eur Ceram Soc.* 2008;28(3):671–678. https://doi.org/10.1016/j.jeurceramsoc.2007.07.013
- 28. Kim KH, Shim KB. The effect of lanthanum on the fabrication of ZrB2-ZrC composites by spark plasma sintering. *Mater Charact*. 2003;50(1):31–37. https://doi.org/10.1016/S1044-5803(03)00055-X
- 29. Ordan'yan SS, Unrod VI. Reactions in the system ZrC-ZrB2. *Sov Powder Metall Met Ceram*. 1975;14(5):393–395. https://doi.org/10.1007/BF00807811
- 30. Sorrell CC, Beratan HR, Bradt RC, Stubican VS. Directional Solidification of (Ti, Zr) Carbide-(Ti, Zr) Diboride Eutectics. *J Am Ceram Soc.* 1984;67(3):190–194. https://doi.org/10.1111/j.1151-2916.1984.tb19740.x

- 31. C. E. Brukl. Ternary Phase Equilibria in Transistion Metal-Boron-Carbon-Silicon Systems
 Systems Part II. Ternary Systems, Volume X. The Zr-Si-C, Hf-Si-C, Zr-Si-B, and Hf-Si-B
 Systems. Wright- Patterson Air Force Base, Ohio: 1966
- 32. King DS, Hilmas GE, Fahrenholtz WG. Plasma arc welding of ZrB2-20 vol% ZrC ceramics. *J Eur Ceram Soc.* 2014;34(15):3549–3557. https://doi.org/10.1016/j.jeurceramsoc.2014.05.011
- 33. Klug FJ. Alumina-Silica Phase Equilibria in the Mullite Region. 1984;59.